Dynamics of singlet excitations in conjugated polymers: Poly(phenylenevinylene) and poly(phenylphenylenevinylene)

B. Mollay
Institut für Physikalische Chemie der Universität Wien, Währingerstraße 42, A-1090 Wien, Austria

U. Lemmer
Fachbereich Physik und Zentrum für Materialwissenschaften, Philipps-Universität Marburg, Renthof 5, D-35032 Marburg, Germany

R. Kersting
Institut für Halbleitertechnik II, Rheinisch-Westfälische Technische Hochschule Aachen, Sommerfeldstrasse 24, D-52056 Aachen, Germany

R. F. Mahrt
Fachbereich Physikalische Chemie und Zentrum für Materialwissenschaften, Philipps-Universität Marburg, Hans-Meerwein-Strasse, D-35032 Marburg, Germany

H. Kurz
Institut für Halbleitertechnik II, Rheinisch-Westfälische Technische Hochschule Aachen, Sommerfeldstrasse 24, D-52056 Aachen, Germany

H. F. Kauffmann
Institut für Physikalische Chemie der Universität Wien, Währingerstraße 42, A-1090 Wien, Austria

H. Bässler
Fachbereich Physikalische Chemie und Zentrum für Materialwissenschaften, Philipps-Universität Marburg, Hans-Meerwein-Strasse, D-35032 Marburg, Germany
(Received 25 April 1994; revised manuscript received 5 July 1994)

The decay of the photoluminescence of the conjugated polymers, poly(phenylenevinylene), poly(phenylphenylenevinylene) (PPPV), and PPPV blended with polycarbonate is measured as a function of the position of the spectral detection window employing frequency-up-conversion and streak-camera techniques. Upon probing at the high-energy side of the inhomogeneously broadened $S_1 \leftarrow S_0$ 0-0 transition, an initial falloff characterized by a $(1/e)$ decay time of about 300 fs is observed. This decay slows down by three orders of magnitude upon shifting the detection window towards lower energies. We present a quantitative analysis of these experimental data by performing simulations of dipole-dipole excitation transfer on a random lattice chain with energetic site disorder. They give evidence for the notion that photon absorption generates neutral excitations undergoing a random walk among segments of the polymer chain with different excitation energies.

I. INTRODUCTION

The nature of optically generated elementary excitations in conjugated polymers as well as their dynamics is currently under debate. The conventional notion has been that these systems behave like one-dimensional (1D) semiconductors tractable in terms of the Su-Schrieffer-Heeger (SSH) Hamiltonian[1] that includes neither Coulomb nor electron correlation effects but invokes strong electron-phonon interaction. Disorder as well as interchain effects are considered to be of secondary importance. The elementary optical excitations are described as free electron-hole pairs, generated with unit quantum efficiency, that rapidly self-localize to form polarons and bipolarons. The former can recombine radiatively giving rise to photoluminescence associated with a Stokes shift that reflects the polaron binding energy. Photoconduction action spectra[2–5] as well as photoinduced absorption experiments[6–8] support this concept.

An alternative model is based upon a molecular approach. Given the fact that the chains in a noncrystalline polymer are not perfectly aligned it appears straightforward to treat a conjugated polymer as an array of subunits. The effective conjugation length of these subunits, L_{eff}, depends on sample perfection and is, concomitantly, subject to statistical variation. The absorption spectrum reflects the inhomogeneously broadened vibronic $S_1 \longleftarrow S_0$ absorption manifold of these subunits, their elementary excitations being Coulomb-bound electron-hole pairs, not different from the elementary excitations of

 ©1994 The American Physical Society

oligomeric model compounds.[9,10] In accord with this, the absorption spectra of partially ordered conjugated polymers, such as stretch-aligned poly(phenylenevinylene) (PPV), reveal a vibronic fine structure and differ from those of their corresponding oligomers by some redshift only.[11] Further support comes from the recent observation that site-selectively excited luminescence spectra of both π- and σ-conjugated polymers reveal little or no Stokes shift indicating that electron-phonon interaction is weak and comparable to that of oligomers.[12,13] Recent theory, moreover, proves that electron-hole interaction has to be taken into account for an adequate description of the linear and nonlinear optical properties.[14,15] Recent experimental results[16,17] support this notion.

The present paper focuses on transient aspects of photoluminescence in PPV-type systems. Following the semiconductor approach there should be rapid intraband relaxation of optically generated free charge carriers towards the band edges followed by polaron formation. These processes should be more or less independent of the primary excitation energy and occur on a subpicosecond time scale. Such ultrafast intraband carrier relaxation processes have been observed in III-V semiconductors.[18,19] In terms of the molecular approach a conjugated polymer should behave like an array of chromophores with statistically varying excitation energy, manifest in the inhomogeneously broadened absorption spectra, among which incoherent energy transport takes place accompanied by time- and energy-dependent electronic relaxation of the excitations towards the tail states of the density of states (DOS).[20] It should give rise to both a redshift of the photoluminescence (PL) spectra with time[21] and a decay pattern that strongly depends on the spectral position at which the PL is probed. The latter phenomena have been observed in recent experiments.[22,23] The present work focuses on a quantitative understanding of the excitation dynamics in PPV-type conjugated polymers in terms of the concept of hopping motion of neutral excitations migrating via dipole-dipole coupling. We present a computational framework[24–26] for rationalizing the spectrally resolved decay of photoluminescence. The role of the computer is (i) to generate Monte Carlo chain configurations and (ii) to calculate the optical dynamics of a migrating excitation based on an energy-space transport master equation. Both site-specific frequency-domain and time-domain solutions, i.e., the spectrum of eigenvalues and the excitation survival probability, are computed. They demonstrate the typical kinetic signature of electronic relaxation in energy-dispersive excitation transfer. The results of the simulation are directly related to the energy-selective luminescence response and are compared to previous and new experimental data. Both simulations and experimental data strongly support the notion that the elementary excitations determining the luminescence behavior are (neutral) excitons undergoing an incoherent random walk among subunits of the polymer chains.

II. EXPERIMENTAL AND RESULTS

The time-resolved photoluminescence experiments are performed on (i) poly(phenylenevinylene) (PPV) films prepared via the precursor route, (ii) spin-coated films of the soluble poly(phenylphenylenevinylene) (PPPV) synthesized via the Heck reaction, and (iii) 1% blend of PPPV and polycarbonate (PPPV/PC). The average chain length of PPV and PPPV is about 400 and 45 repeat units, respectively.

The temporal evolution of the luminescence is measured at variable spectral positions within the inhomogeneously broadened $S_1 \leftarrow S_0$ 0-0 absorption band. To resolve ultrafast relaxation processes, femtosecond (fs) luminescence up-conversion spectroscopy is applied.[27] For these experiments we use a Kerr lens mode-locked Ti-sapphire laser producing 150 fs pulses at 1.56 eV and a repetition rate of 76 MHz. The samples are excited by frequency-doubled laser pulses at 3.12 eV implying that the initial state is a vibronically excited S_1 state. The excitation power was reduced to 0.8 mW on a spot size diameter of about 100 μm to avoid nonlinear annihilation processes and sample degradation. Luminescence emitted from the sample is focused dispersion-free with a mirror optic onto a nonlinear optical crystal of β–barium borate (BBO). Sum frequency light is generated if the luminescence and the reference pulse (1.56 eV) temporally overlap within the crystal. This signal is dispersed by a monochromator and detected by a single photon counting system. The temporal evolution of the luminescence is mapped by delaying the reference pulse with respect to the pulse exciting the sample. The time resolution is limited by the pulse width of the laser and the group velocity dispersion within the BBO crystal between luminescence and reference pulse. For the spectral range investigated in the present measurements the time resolution of the setup is between 160 fs at 1.8 eV and 300 fs at 2.8 eV. The energy resolution of the system is limited by the spectral width of the laser pulses of about 15 meV and the resolution of the monochromator of about 20 meV.

To record PL decays within the time domain 20 ps to 2 ns we use a tunable coumarin 102 dye laser, synchronously pumped by a frequency-tripled mode-locked Nd:YLF (where YLF is yttrium lithium flouride) laser providing 7 ps laser pulses for excitation. The output is

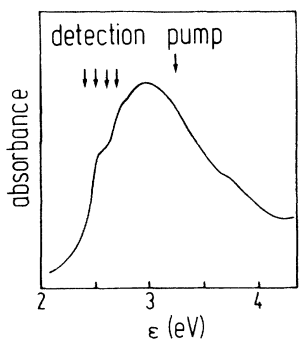

FIG. 1. Absorption spectrum of a PPV film. Arrows indicate luminescence excitation and detection energies, respectively.

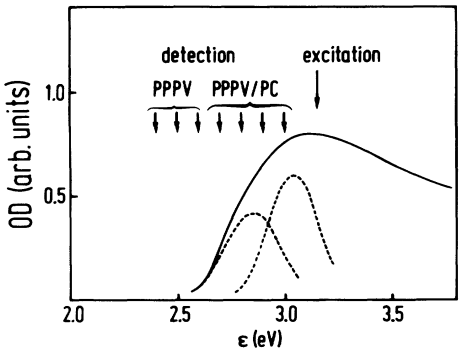

FIG. 2. Absorption of PPPV in the form of either a bulk film or a 1% blend with polycarbonate. Dashed curves represent the inhomogeneously broadened $S_1 \leftarrow S_0$ 0-0 and 1-0 transitions, respectively. Arrows indicate luminescence excitation and detection energies.

reduced to 1 mW (at a repetition rate of 76 MHz) and focused onto a spot size of 1.5 mm in diameter. The luminescence is passed through a 0.64 m monochromator and detected by a streak camera with 20 ps time resolution. These experiments are performed at room temperature and at 10 K, respectively. The spectral positions at which the PL decay is monitored are indicated in the related absorption spectra shown in Figs. 1 and 2.

While the PPV absorption spectrum displays vibronic structure that allows locating the center of the inhomogeneously broadened $S_1 \leftarrow S_0$ 0-0 transition at 2.55 eV, no such structure is seen in the PPPV spectrum whose shape is the same for the bulk material and the blend. A straightforward reason is the larger degree of disorder introduced by the bulky substituent that disturbs chain alignment. As a consequence the average effective conjugation length L_{eff} is shorter and larger variations of L_{eff} translate into a larger spread of $S_1 \leftarrow S_0$ transition energies. Based upon the knowledge of the vibrational energies of the repeat unit, which are virtually the same as those of the PPV unit, one can do a crude deconvolution of the absorption spectrum locating the $S_1 \leftarrow S_0$ 0-0

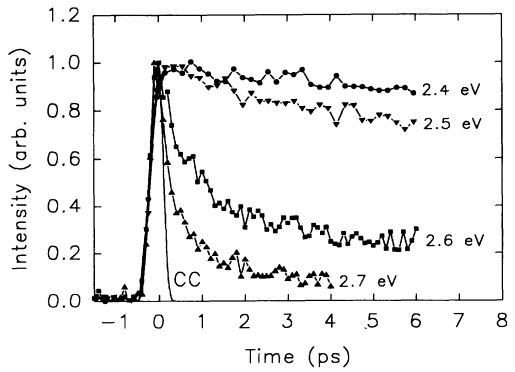

FIG. 3. Temporal decay of the photoluminescence of a PPV film probed at variable detection energies at 295 K. CC (solid line) denotes the cross correlation of exciting and reference pulse.

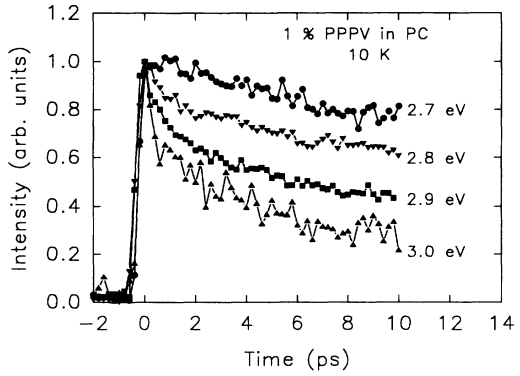

FIG. 4. Normalized PL decay in a PPPV/PC blend at different detection energies.

band center at 2.83 eV and yielding a Gaussian width of $\sigma = 0.13$ eV as compared to $\sigma = 0.09$ eV in the case of PPV.

PL-decay curves recorded for PPV and PPPV/PC employing the up-conversion technique are presented in Figs. 3 and 4. The facts that (i) even during excitation no significant luminescence is observed near the pump photon energy and (ii) the luminescence recorded at various probe energies rises quasi-instantaneously with the laser pulse indicate that vibronic cooling of the excited state occurs on a time scale shorter than our time resolution. It is obvious that this fast relaxation process erodes any site selectivity if initially existing and guarantees that at the beginning of the luminescence decay experiment the electronic excitations are randomly distributed within the manifold of the zero vibronic S_1 states.

The luminescence transients measured in the streak-camera experiments on bulk PPPV films (Fig. 5) at the very tail of the absorption spectrum confirm that the prolongation of the decay process continues down to the lowest detection energies until ultimately a decay time of several hundred ps is attained.

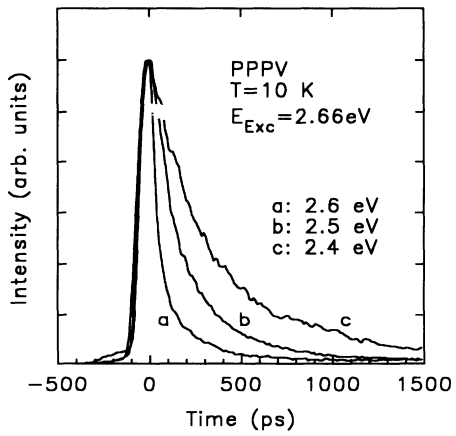

FIG. 5. Photoluminescence decay of a PPPV film probed at the tail of the absorption spectrum.

III. COMPUTATIONAL EXPERIMENTS

A. Model and formalism

The method[24–26] which we have modified here to mimic dispersive excitation transfer in PPPV consists of a Monte Carlo–master equation hybrid technique that (i) generates chain configurations and (ii) solves the incoherent excitation hopping problem by calculating the relaxation profile of the energy-dependent survival probability that relates directly to the observed luminescence response. The chain is a simple hard-sphere model synthesized by a self-avoiding random walk on a cubic lattice. Typically, the chain carries 50 sites located at the intersections of the bond vectors that mimic the typical sequence of aryl-vinyl repeat units in PPPV. Chains consisting of (i) pure donors and (ii) donors and traps, randomly attached to the chain, are investigated.

The dispersion of donor site energies, i.e., the statistical fluctuation of conjugation lengths, is modeled in terms of a Gaussian distribution

$$N(\epsilon;\sigma) = 1/\sqrt{2\pi\sigma}\, e^{-(\epsilon-\bar{\epsilon})^2/2\sigma^2} \tag{1}$$

with $\bar{\epsilon}$ being the central mean and the standard deviation σ defining the width of the distribution. Traps are assumed to lie sufficiently below the Gaussian DOS to prevent trap release.

For the calculation of site-to-site transition rates between donors i and j an energy-dependent coupling term factorized into space- and energy-dependent contributions is chosen:

$$\gamma_{ij}^{DD} = \eta_0^{DD} \left(\frac{d^{DD}}{|r_i - r_j|} \right)^6 \vartheta(\epsilon_i, \epsilon_j) \ . \tag{2}$$

$\vartheta(\epsilon_i, \epsilon_j)$ is a Boltzmann-type weighting factor

$$\vartheta(\epsilon_i, \epsilon_j) = \begin{cases} \exp\left[-(\epsilon_j - \epsilon_i)/kT\right], & \epsilon_j > \epsilon_i \\ 1, & \epsilon_j \le \epsilon_i \end{cases} \tag{3}$$

that controls uphill processes ($\epsilon_j > \epsilon_i$). Downhill processes within the site ensemble are assumed to be temperature independent and transitions from donors to traps are considered to be independent of the trap depth [$\vartheta(\epsilon_i, \epsilon_j) = 1 \ \forall \ i, j > n_D$]. The spatial term describes dipolar coupling[28] with a minimum site-to-site distance d^{DD} between donors and a transfer rate η_0^{DD} which equals γ_{ij}^{DD} if $|r_i - r_j| = d^{DD}$ (nearest-neighbor transition rate). The same Förster-type functional relationship is used for the calculation of the trapping processes (γ_{ij}^{DT}). The entire set of dipolar interactions is taken into account and no cutoff has been applied.

Based upon these assumptions dispersive transport of excitations with infinite lifetime is modeled by an asymmetric master equation. Hence, for a particular random chain with n sites the equation of motion for incoherent transport of a site-oriented (molecular) excitation is

$$\dot{\mathbf{p}}(t) = \mathbf{W}\mathbf{p}(t); \quad \mathbf{W} = [W_{ij}]_{n\times n} \ , \tag{4}$$

where $\mathbf{p}(\mathbf{t})$ is the n-dimensional excitation vector containing the site population elements $p_i(t)$ and $\mathbf{W}$ is the energy-dependent relaxation matrix

$$\mathbf{W} = \mathbf{W}(\{\epsilon_i | i = 1, \ldots, n_D\}, \{\mathbf{r}_j | j = 1, \ldots, n\}) \ , \tag{5}$$

with elements

$$W_{ij} = (1 - \delta_{ij})\gamma_{ji} - \delta_{ij} \sum_{\substack{l=1 \\ l\neq i}}^{n} \gamma_{il} \ . \tag{6}$$

The time behavior of the site occupation probability $p_i(t)$ has the general form

$$p_i(t) = \sum_{j=1}^{n} v_{ij} \sum_{l=1}^{n} p_l(0) v_{jl}^{-1} e^{\lambda_j t}, \quad i = 1, \ldots, n \ , \tag{7}$$

with eigenvalues λ_j and eigenvectors v_{ij} (v_{jl}^{-1}, inverse) that follow from

$$[\mathbf{W} - \lambda_j \mathbf{I}]\, \mathbf{v}_j = \mathbf{0}, \quad j = 1, \ldots, n \ . \tag{8}$$

Under conditions of a spectrally broad δ-shaped optical pulse as realized in experiment (Sec. II) the ensemble of excitable sites (n_D donor sites) is uniformly populated at $t = 0$ and the initial boundaries read

$$p_i(0) = \begin{cases} 1/n_D, & i = 1, \ldots, n_D \\ 0, & i = n_D + 1, \ldots, n \ . \end{cases} \tag{9}$$

By combining Eqs. (7) and (9) we obtain

$$p_i(t) = 1/n_D \sum_{j=1}^{n} v_{ij} \sum_{l=1}^{n_D} v_{jl}^{-1} e^{\lambda_j t}, \quad i = 1, \ldots, n \ . \tag{10}$$

Energy-selective detection as performed in our experiments implies that only a subset of donor sites with energies in a distinct interval $\Delta\hat{\epsilon}$ (luminescence window) is probed. The probability that an electronic excitation at time t is found in a subensemble with site energy $\Delta\hat{\epsilon}$ is therefore

$$p(t; \Delta\hat{\epsilon}) = \sum_{\substack{i=1 \\ \epsilon_i \in \Delta\hat{\epsilon}}}^{n_D} p_i(t) \ , \tag{11}$$

which is directly related to the luminescence response collected in the spectral window. By substituting Eq. (10) into (11) and changing the order of summation the energy-specific excitation survival function can be written as

$$p(t; \Delta\hat{\epsilon}) = \sum_{j=1}^{n} 1/n_D \sum_{\substack{i=1 \\ \epsilon_i \in \Delta\hat{\epsilon}}}^{n_D} v_{ij} \sum_{l=1}^{n_D} v_{jl}^{-1} e^{\lambda_j t} \ , \tag{12}$$

which is an n-term exponential series

$$p(t; \Delta\hat{\epsilon}) = \sum_{j=1}^{n} \mathcal{A}_j(\Delta\hat{\epsilon}) e^{\lambda_j t} \tag{13}$$

with amplitudes defined by

$$\mathcal{A}_j(\Delta\hat{\epsilon}) := 1/n_D \sum_{\substack{i=1 \\ \epsilon_i \in \Delta\hat{\epsilon}}}^{n_D} v_{ij} \sum_{l=1}^{n_D} v_{jl}^{-1}, \quad j = 1, \ldots, n \,. \quad (14)$$

The function $p(t;\Delta\hat{\epsilon})$ [Eq. (13)] depends on both the spatial coordinates of the entire site ensemble and the self-energies of the whole set of donor sites [cf. Eq. (2) and Eq. (5)], for a particular configuration s. The statistical mechanical average over site energies and N chain configurations is therefore

$$\begin{aligned}\langle p(t;\Delta\hat{\epsilon})\rangle &= \frac{1}{N}\sum_{s=1}^{N} p^{(s)}(t;\Delta\hat{\epsilon}) \\ &= \frac{1}{N}\sum_{s=1}^{N}\sum_{j=1}^{n} \mathcal{A}_{j,s}(\Delta\hat{\epsilon}) e^{\lambda_{j,s}t} \,. \end{aligned} \quad (15)$$

This is an infinite number of independent configurations due to the continuous (Gaussian) energy distribution [Eq. (1)]. The number of terms in the exponential series is thus *unbounded above*. Since the eigenvalues of the transition matrix $\mathbf{W}$ are negative, this yields for $N \longrightarrow \infty$

$$\begin{aligned}\langle p(t;\Delta\hat{\epsilon})\rangle_{\mathrm{ex}} &= \lim_{N\to\infty} \frac{1}{N}\sum_{s=1}^{N}\sum_{j=1}^{n} \mathcal{A}_{j,s}(\Delta\hat{\epsilon}) e^{\lambda_{j,s}t} \\ &= \int_0^\infty \langle \Phi(\omega;\Delta\hat{\epsilon})\rangle e^{-\omega t} d\omega \end{aligned} \quad (16)$$

with

$$\omega := |\lambda| \,. \quad (17)$$

The energy-selective excitation survival function $\langle p(t;\Delta\hat{\epsilon})\rangle_{\mathrm{ex}}$ is thus directly related to the eigenvalue spectrum $\langle \Phi(\omega;\Delta\hat{\epsilon})\rangle$ via the Laplace transform and, vice versa, $\langle \Phi(\omega;\Delta\hat{\epsilon})\rangle$ is the inverse Laplace transform of relation (16).

In practical calculation only a finite number of chain realizations can be generated in the averaging procedure, so that the approximate solution to the exact expression in Eq. (16) is better the larger the number of superpositions. In order to obtain a satisfactory approximation to $\langle \Phi(\omega;\Delta\hat{\epsilon})\rangle$ eigenvalues $\lambda_{j,s}$ numerically calculated for each configuration are assigned to the intervals $[\tilde{\omega}_i, \tilde{\omega}_i + \Delta\omega_i]$ which will be replaced by $\omega_i := \tilde{\omega}_i + \Delta\omega_i/2$. The sum in Eq. (15) can then be approximated by

$$\sum_{s=1}^{N}\sum_{j=1}^{n} \mathcal{A}_{j,s}(\Delta\hat{\epsilon}) e^{\lambda_{j,s}t} \approx \sum_{i=1}^{m} \sum_{\substack{j,s \\ -\lambda_{j,s}\in\Delta\omega_i}} \mathcal{A}_{j,s}(\Delta\hat{\epsilon}) e^{-\omega_i t} \quad (18)$$

(m-fold discretization of the ω axis), and by using the definition

$$\sum_{\substack{j,s \\ -\lambda_{j,s}\in\Delta\omega_i}} \mathcal{A}_{j,s}(\Delta\hat{\epsilon})/N =: \langle \tilde{\Phi}_i(\Delta\hat{\epsilon})\rangle \quad (19)$$

Eq. (15) takes the form

$$\langle p(t;\Delta\hat{\epsilon})\rangle \approx \sum_{i=1}^{m} \langle \tilde{\Phi}_i(\Delta\hat{\epsilon})\rangle e^{-\omega_i t} \,, \quad (20)$$

which is the discrete approximation to the exact solution [Eq. (16)]. Typically, 10^4 configurations plus associated master equation solutions are computed to achieve precise, statistical mechanical averages for relaxing optical excitations, in both the frequency and time domains. The eigenvalues $\lambda_{j,s}$ and amplitudes $\mathcal{A}_{j,s}(\Delta\hat{\epsilon})$ necessary for the construction of $\langle \tilde{\Phi}_i(\Delta\hat{\epsilon})\rangle$ and $\langle p(t;\Delta\hat{\epsilon})\rangle$ are solved numerically with the help of standard diagonalization routines (NAG library) based on the QR algorithm.[29]

Recall that $\langle p(t;\Delta\hat{\epsilon})\rangle$ is the survival probability for excitations with infinite intrinsic lifetime τ_0. Since in a hopping process $\langle p(t;\Delta\hat{\epsilon})\rangle$ and the radiative term $(\exp[-t/\tau_0])$ factorize, $\langle p(t;\Delta\hat{\epsilon})\rangle$ is directly proportional to the energy-selective δ-pulse luminescence response of the corresponding site subensemble, i.e.,

$$\begin{aligned} I(t;\Delta\hat{\epsilon}) &\propto e^{-t/\tau_0}\langle p(t;\Delta\hat{\epsilon})\rangle \\ &\propto e^{-t/\tau_0}\sum_{i=1}^{m}\langle \tilde{\Phi}_i(\Delta\hat{\epsilon})\rangle e^{-\omega_i t} \,. \end{aligned} \quad (21)$$

The initial boundaries of our experiments require the assumption of a rigorous (δ-pulse) broadband excitation, to ensure that the entire set of diagonally disordered donor sites is randomly excited at $t = 0$ [cf. condition (9)]. The initial (absolute) intensity of energy-selective luminescence profiles thus depends on the spectral position of the interrogated sites which is governed by the Gaussian density of states $N(\epsilon)$. For a spectral detection window of width $\sigma_D/2$ used in these calculations the initial value is

$$I(0;\Delta\hat{\epsilon}) \propto \langle p(0;\Delta\hat{\epsilon})\rangle = \int_{\epsilon-\sigma_D/4}^{\epsilon+\sigma_D/4} f(\epsilon)\, d\epsilon \,. \quad (22)$$

We will demonstrate these functional relationships in the following simulations.

B. Results

In the following calculations we assume the DOS [Eq. (1)] to be located at $\bar{\epsilon} = 0$. Its width is characterized by a reduced parameter $\hat{\sigma} := \sigma/kT$ and we express the energetic position of the donor site subensemble in units of σ, $\Delta\hat{\epsilon} := \Delta\epsilon/\sigma$. Rectangular spectral packets are used for the energy-selective probing of the donor subset with a typical energetic width $\Delta\epsilon = \sigma_D/2$ for all simulations which is comparable to or larger than the experimental. The absolute value of σ_D (30 meV) is comparable to the spectral resolution in the experiment.

The variables ω and t are normalized to the nearest-neighbor donor-trap transition rate η_0^{DT} [Eq. (2)] and $1/\eta_0^{DT}$, respectively, and the (dimensionless) coupling strength r (in units of η_0^{DT}) has been kept constant in all computations, $r = \eta_0^{DD}/\eta_0^{DT} = 1$. A logarithmic display of the eigenvalues spectra $\langle \tilde{\Phi}_i(\Delta\hat{\epsilon})\rangle$ is chosen, as the spectra generally cover several decades in ω_i space.

The calculated temporal evolution of the survival probability $\langle p(t;\Delta\hat{\epsilon})\rangle$ of excitations generated within the DOS by a uniform δ pulse is given in Fig. 6. The results refer to chains containing 45 donors and five traps for two different reduced widths $\hat{\sigma} = 3$ (solid lines) and $\hat{\sigma} = 20$

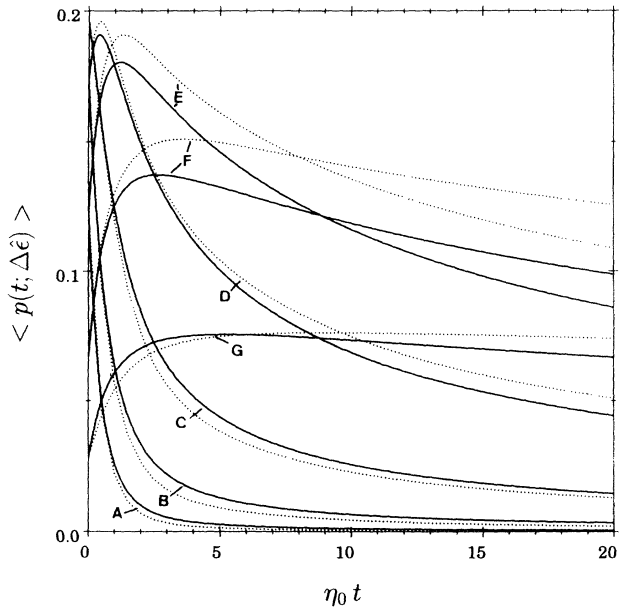

FIG. 6. Excitation survival probability $\langle p(t;\Delta\hat{\epsilon})\rangle$ for different detection energies $\Delta\hat{\epsilon} = \Delta\epsilon/\sigma = 1$ (A), 0.5 (B), 0 (C), -0.5 (D), -1 (E), -1.5 (F), and -2 (G), respectively. Solid and dotted patterns refer to $\hat{\sigma} = \sigma/kT = 3$ and 20, respectively. Chains (10^4 realizations) contain 45 donor sites and five traps, outside the DOS.

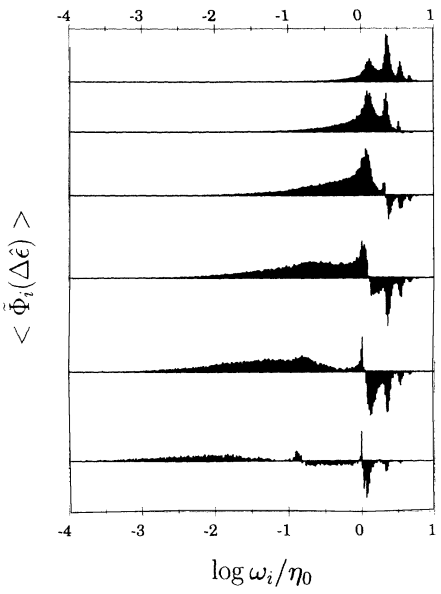

FIG. 7. Structure of eigenvalue spectra $\langle\Phi_i(\Delta\hat{\epsilon})\rangle$ as a function of varying detection energies, from top to the bottom: $\Delta\hat{\epsilon} = \Delta\epsilon/\sigma = 1$, 0.5, 0, -0.5, -1, and -2, respectively ($\hat{\sigma} = \sigma/kT = 3$). The spectra represent the inverse Laplace transform of the $\langle p(t;\Delta\hat{\epsilon})\rangle$ curves in Fig. 6 (solid lines).

(dotted curves), respectively. The curves correspond to $\Delta\hat{\epsilon} = 1$ (A), 0.5 (B), 0 (C), -0.5 (D), -1 (E), -1.5 (F), and -2 (G), respectively. For $\Delta\hat{\epsilon} = 1$, 0.5, and 0, respectively, $\langle p(t;\Delta\hat{\epsilon})\rangle$ appear to be pure decay functions and they show—except at very short times—a pronounced nonexponential behavior if plotted on a semilogarithmic scale. As shown in Fig. 6, for $\hat{\sigma}$ not too low and for high-energetic subsets of sites [$\Delta\hat{\epsilon} = 1$ (A), 0.5 (B), 0 (C)], downhill depopulation plays the dominant role and causes the rapid decay. Nevertheless, even these profiles contain small contributions of rise components giving rise to formally *negative* amplitudes in the eigenvalue spectra $\langle\tilde{\Phi}_i(\Delta\hat{\epsilon})\rangle$ of Fig. 7.

The entire set of $\langle\tilde{\Phi}_i(\Delta\hat{\epsilon})\rangle$ underlying the (dotted) time-domain curves of Fig. 6 is displayed in Fig. 7, for $\hat{\sigma} = 3$ and different values of $\Delta\hat{\epsilon}$. The typical fine structure of such spectra reflects directly the number of nearest-neighbor donor-trap contacts in our polymer model[24] which will not be discussed here. Note that only in case of high energies ($\Delta\hat{\epsilon}$, spectrum at the top) does $\langle\tilde{\Phi}_i(\Delta\hat{\epsilon})\rangle$ consist of positive amplitudes only and thus give rise to pure decay terms in the evolution of $\langle p(t;\Delta\hat{\epsilon})\rangle$ (curve A in Fig. 6). For $\Delta\hat{\epsilon} = 0.5$ and 0.0 contributions of significant negative amplitudes exist which cannot be observed as the respective rise terms in the time-domain solutions (curves B and C in Fig. 6), at least, on the (reduced) long-time axis chosen in this presentation. Generally, negative and positive amplitude spectra are caused by the dominance of gain and loss processes, respectively. Spectral position, intensity, width, and size of the amplitudes thus strongly depend on the energy of the site subensemble probed in the simulation. The lower-energetic the luminescence window, the more predominant become the negative amplitudes. This leads to increasing admixtures of rise phases in the time domain (Fig. 6, curves D, E, F, and G) corresponding to $\Delta\hat{\epsilon} = -0.5$, -1, -1.5, and -2, respectively. Note the difference in the initial values of $\langle p(0;\Delta\hat{\epsilon})\rangle$ and in population maxima of these curves as well as the different times at which these maximum values are attained.

At low temperatures ($\hat{\sigma} = 20$, dotted curves in Fig. 6) the survival probabilities for excitations at high energies decay faster (curves A, B, and C), because thermal uphill promotion is negligible. Vice versa, there is a characteristic slowing down of the rise component and the attainment of a plateau for site subensembles probed at low detection energies ($\Delta\hat{\epsilon} = -2$, curve G).

The effect of funneling migrating excitation into low-energy tail states is even more pronounced in a trap-free donor site ensemble. The dotted patterns in Fig. 8 refer to $\langle p(t;\Delta\hat{\epsilon})\rangle$ in the absence of traps, whereas the solid profiles correspond to the excitation trapping dynamics as already discussed in Fig. 6 ($\hat{\sigma} = 3$). Again, the spectral detection windows have been chosen to be $\Delta\hat{\epsilon} = 1$ (A), 0.5 (B), 0 (C), -0.5 (D), -1 (E), -1.5 (F), and -2 (G). In particular, the site-subensembles in the ultimate low-energy wing centered at $\Delta\hat{\epsilon} = -1.5$ (F) and -2 (G) show typical migrative population patterns which, at least on this time scale, are not counterbalanced by predominant decay events. It becomes apparent from these profiles that the waiting times of the hopping exciton gradually increase in the course of excitation energy cas-

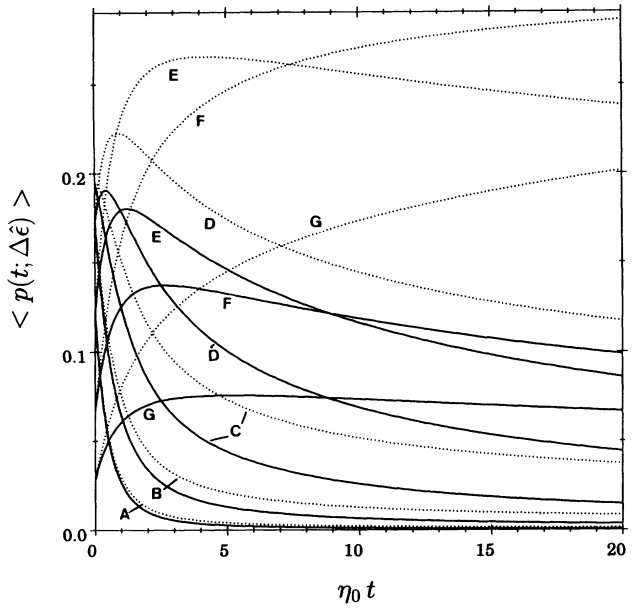

FIG. 8. $\langle p(t;\Delta\hat{\epsilon})\rangle$ in presence (solid curves; see also Fig. 6) and in the absence of traps (dotted patterns) for detection energies $\Delta\hat{\epsilon} = \Delta\epsilon/\sigma = 1$ (A), 0.5 (B), 0 (C), -0.5 (D), -1 (E), -1.5 (F), and -2 (G), respectively. The width has been chosen to be $\hat{\sigma} = \sigma/kT = 3$. See the text for details.

cading and transport will be more and more slowed down. This behavior is the reason for the significant *freezing-in* of excitation transfer in energetically and spatially disordered random systems.[30] In absence of a trap the termination of a hopping cascade is reached if the excitation is surrounded by energetically higher states, which is the better fulfilled, the lower the energy of the probing window and the lower the temperature is. Note that in the trap-free system the energy-averaged survival function in the asymptotic limit is $\langle\langle p(t=\infty)\rangle\rangle = 1$.

IV. DISCUSSION

The variation of the characteristic decay time of the luminescence by almost three orders of magnitude upon redshifting the detection window, the accompanied redshift of the emission spectrum reported earlier,[21] and the nonexponential decay pattern combined with the independence of these effects of pump intensity are characteristic features of spectral relaxation of neutral excitations within an inhomogeneously broadened density of states. In view of the obvious correspondence between experimental (Sec. II) and computational data (Sec. III) we shall start this discussion by comparing both in a quantitative manner. The question of central concern in the forthcoming analysis is therefore the availability of a theoretically sound time-domain trial function for examining both experimental $I(t)$ and simulated $\langle p(t;\Delta\hat{\epsilon})\rangle$ curves. For incoherent excitation transfer in *random* media the stretched exponential form of the Kohlrausch-Williams-Watts (KWW) function[31]

$$I(t) = I_0 \exp[-(t/t_0)^{\beta}] \tag{23}$$

has been shown to be the natural output of a variety of theoretical treatments. The extended exponential is the logical result of parallel, i.e., unconstrained, relaxation steps[32] but it is associated with a picture of hierarchically constrained models,[33] as well. Thus, on the one hand, the KWW law has been recovered in a model of independent single-step processes; on the other hand, it has been obtained in sequential, multistep processes on temporally, spatially, and energetically disordered structures,[34] thereby reflecting the distributed nature of microscopic relaxation channels in randomly disordered materials, in general. In order to examine the validity of such a law for our data, it is useful to replot our temporal decay patterns. Should $I(t)$ obey a KWW behavior [Eq. (23)], a double logarithmic plot of $\ln I_0/I(t)$ versus t/t_0 should yield a straight line with slope β (β and t_0 describing the dispersion and the time scale, respectively). For converting the data of Fig. 6 it was assumed that I_0 is determined by the extrapolation of the decay portion of $I(t)$ towards $t = 0$. Analyzing the decay portion of the simulation data for the spectrally resolved time-dependent luminescence shown in Fig. 6 [$\langle p(t;\Delta\hat{\epsilon})\rangle \propto I(t)$] reveals significant deviations from KWW behavior [Figs. 9(a) and 9(b)].

For short times the slope of $\log_{10}\ln I_0/I(t)$ vs $\log_{10} t/t_0$ plots approaches unity, which is equivalent to exponential decay. Only in the asymptotic, long-time limit is KWW-like behavior with a limiting value $\beta = 0.4$ attained, whereas in the intermediate regime a curved region is obtained—equivalent to a formal time dependence of the exponent β. This deviation is, last but not least, not so surprising, since the KWW law is, in general, the statistical mechanical average of microscopic relaxations for *random*, infinite systems, while the site ensemble in the present test system has a finite, *nonrandom* structure.

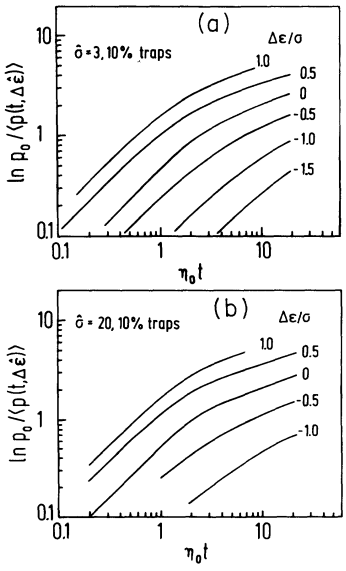

FIG. 9. $\ln I_0/I(t)$ versus $\eta_0 t$ (from Fig. 8) plotted on a double logarithmic scale. (a) $\hat{\sigma} = 3$, (b) $\hat{\sigma} = 20$.

Notably at short times the decay is virtually independent of temperature. The main effect of lowering the temperature, or, equivalently, increasing the degree of energetic disorder, is that turnover to nonexponential decay behavior starts earlier. The same trend is seen if the spectral detection window is shifted towards lower energies and/or if traps are removed from the system. The qualitative understanding of this result is straightforward. At the beginning of its motion an excitation will execute nearest-neighbor jumps only. Given the discrete chain structure these occur with a rate proportional to the probability that the sites next to an excited site have lower energies and, consequently, can act as energy acceptors. If the spectral detection window is at the high-energy tail of the density of states the average number of acceptors is given by the coordination number of a random chain, which is close to 2. In accord with this argument, the extrapolated $1/e$ decay time t_0 inferred from the initial slope of the high-energy $\langle p(t, \Delta\hat{\epsilon})\rangle$ is $(2\eta_0)^{-1}$, η_0^{-1} being the minimum nearest-neighbor transfer time. As $\Delta\hat{\epsilon}$ decreases, the probability that a site next to a donor is downhill in energy decreases. Consequently, both the extrapolated $1/e$ decay rate and the amplitude of the initial exponential decay component must decrease in proportion to the number of nearest-neighbor acceptor states having lower energy. At the same time the decay domain that is controlled by jumps to non-nearest-neighbors starts earlier, the deviation from exponential decay behavior reflecting the distribution of transfer rates. Increasing disorder, i.e., lowering the temperatures, slows down the transfer process without changing its temporal pattern, though. The asymptotic $\langle p(t; \Delta\hat{\epsilon})\rangle$ behavior is KWW-like, the exponent β being between 1/2 and 1/3 as expected for Förster transfer from a random ensemble of donors to a dilute array of acceptors in the 3D and the 2D case, respectively.[34] In a system composed of real chromophores with finite excited state lifetime the $t \to \infty$ behavior of $I(t)$ should merge into an exponential decay reflecting intrinsic decay of excitations.

The overall temporal decay pattern of the donor sites located in a certain energy slice within the DOS is controlled by population from higher-lying states and relaxation towards lower-lying states. Since, on the average, the former process is faster the competition between both processes should yield $\langle p(t; \Delta\hat{\epsilon})\rangle$ curves featuring maxima that become more pronounced as $\Delta\hat{\epsilon}$ is lowered. This fact is seen in the simulation (Figs. 6 and 8). It is less pronounced in systems containing nonfluorescent traps because trap capturing competes with the accumulation of excitations within the tail states of the DOS.

Qualitative comparison of experimental $I(t; \Delta\hat{\epsilon})$ curves (Figs. 3, 4, and 5) with computed density profiles $\langle p(t; \Delta\hat{\epsilon})\rangle$ for systems with and without traps outside the intrinsic DOS (Fig. 8) indicates overall agreement on the premise that the experimental systems do contain traps. Observing only a short rise component of the luminescence signal probed at the detection energies indicates that only a fraction of the excitations that relax from higher states in the DOS accumulate in the bottom states of the intrinsic DOS, the remainder being scavenged by nonfluorescent traps. This is in accord with recent studies of the spectrally integrated luminescence decay.[23] It has been found that the luminescence decay of PPV is non-exponential, featuring an initial $1/e$ decay time of the order of 100 ps and a long-lasting tail. Both the temperature dependence of the decay as well as its sensitivity to morphology and chemical substitution (e.g., PPV versus PPPV) strongly suggest that this is an extrinsic rather than an intrinsic property and has to be rationalized in terms of trapping by accidental impurities, such as residues of precursor, catalyst, or uv photo-oxidation products.[35] Comparing the experimental $I(t, \epsilon)$ data with computations indicates that the trap concentration has to be of the same order, i.e., 10%, as that used for calculating the data of Figs. 6 and 8. At first glance this appears unrealistic. However, one has to take into account that the sites are idealized point sites in simulation, while the chromophore in a conjugated polymer is a subunit of the chain comprising typically ten repeat units. Since an excitation will be spread out over the entire subunit, it will sample all trapping possibilities due to impurity molecules located within a tube surrounding the excited subunit. Consequently a 10% trap concentration in simulation corresponds to a trap concentration of order 1% in the real sample. Further, one has to take into account that Förster radii for donor-acceptor transfer are usually larger than those for donor-donor transfer because of improved spectral overlap. Therefore fewer hops are needed in the real sample as compared to the computer system in order to account for the same trapping efficiency. It is gratifying to note that recent energy transfer studies on dye-doped PPPV (Ref. 36) suggested that the material contained approximately 1% of non-fluorescent traps.

One problem that is, in principle, encountered when comparing experimental with computed decay curves is that the vibronic replicas of emissions from states near the center of the DOS contribute to the emission recorded at lower detection energies. In view of the rapid depopulation of higher-lying states this effect can only give a marginal contribution towards the initial position of the PL rise component recorded at lower detection energies. It is certainly insufficient to invalidate the above conclusion that the existence of traps is needed to explain the short-time behavior of PL at low detection energies.

For analyzing luminescence decay in terms of the energy transfer concept $I(t)$ curves have been replotted as $\log_{10}\ln I_0/I(t)$ vs $\log_{10} t$ to allow direct comparison with the simulation results. It is further necessary to locate the spectral detection window on an energy scale normalized to the width σ of the DOS and centered at the maximum of the $S_1 \leftarrow S_0$ 0-0 transition, which occurs at 2.55 eV and 2.83 eV, in the case of PPV and PPPV/PC, respectively. Based upon the values σ(PPV) = 0.09 eV and σ(PPPV/PC)= 0.13 eV, detection energies of $\epsilon = 2.7$ eV, 2.6 eV, and 2.5 eV translate into $\Delta\epsilon = 1.7, 0.5$, and -0.5, respectively, in the case of PPV, while for PPPV/PC and PPPV detection energies $\epsilon = 3.0, 2.9, 2.8, 2.7, 2.6, 2.5$, and 2.4 eV are equivalent to $\Delta\hat{\epsilon} = 1.3, 0.53, -0.23, -1.0, -1.76, -2.5$, and -3.3, respectively.

Comparing the decay patterns of PPV as well as of

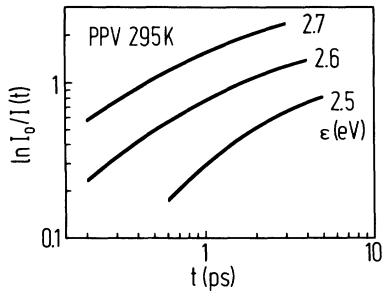

FIG. 10. Smoothed decay curves of the PL in PPV (from Fig. 3) replotted on a double logarithmic $\ln I_0/I(t)$ versus time scale.

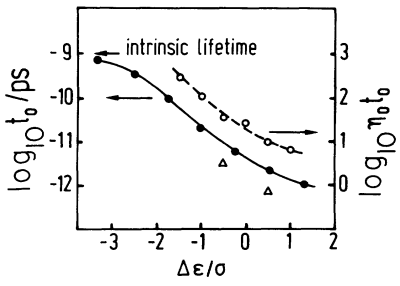

FIG. 12. Dependence of the extrapolated $1/e$ decay time of the initial portion of the luminescence decay of PPPV/PC and PPPV (solid circles) and PPV (triangles) on the position $\Delta\epsilon/\sigma = \Delta\hat{\epsilon}$ of the spectral detection windows. The result of the simulation (open circles, right ordinate) is included for comparison.

PPPV/PC and PPPV plotted on a KWW-type scale (Figs. 10 and 11) with Fig. 9 indicates general agreement. In all cases the experimental profiles at intermediate times strongly deviate from the KWW form, but the $I(t)$ patterns approach a stretched exponential behavior with $\beta \approx 0.4$ in the long-time limit. Probing the emission at the very tail of the DOS ($\epsilon = 2.4$ eV for PPPV) even reveals turnover to exponential decay for times $t \geq 0.8$ ns bearing out a decay time of about 1 ns which is close to the intrinsic decay time of an oligomeric model compound.[37] In the short-time limit $\log_{10}\ln I_0/I(t)$ vs $\log_{10}t$ curves bend over to ultimately approach a slope of 1, indicating that the decay process becomes first order. The asymptotic limit is not fully reached with the high-energy $I(t)$ curves of PPV and PPPV/PC because in this case the (experimental) decay time becomes comparable to the time resolution of the setup. Deviations seen with the 2.7 eV curve of PPPV/PC, on the other hand, are due to difficulties in determining I_0 because in that case luminescence buildup is important at early times.

From the asymptotic short-time limit the decay time t_0 of the initial exponential component of the decay process can be determined and compared with the simulation result. Figure 12 presents data for t_0 as a function of normalized detection energy $\Delta\epsilon/\sigma = \Delta\hat{\epsilon}$ in comparison with simulation data normalized to the nearest-neighbor transfer time η_0^{-1} for excitation transport along the lattice chain. The agreement between computation and experiment is obvious. This allows one to determine an absolute value for the nearest-neighbor transfer time η_0^{-1}, once the number of nearest neighbors in the real sample is known. Assuming that the topology in PPPV/PC resembles that in the molecular chain, i.e., each site has two nearest neighbors, one arrives at $\eta_0^{-1} \approx 2 \times 10^{-12}$ s, equivalent to a minimum dwell time of 1 ps on a site with twofold coordination. The data points for PPV indicate that in this system the initial transfer process occurs by a factor of 3 faster than in PPPV/PC. This is likely to be the consequence of a larger coordination number in the bulk system.

If one makes the assumption that the fastest energy transfer processes occur across an intermolecular distance of 6 Å one can translate η_0 into a Förster radius R_0 via

$$\eta_0 = \tau_0^{-1}\,(R_0/a)^6 \tag{24}$$

where τ_0 is the intrinsic lifetime (1 ns). This yields $R_0 \approx$ 18 Å which is a typical value for singlet energy transfer among donor molecules.

The dwell time of an excitation on a PPV site at the top of the DOS ($\simeq$ 300 fs) is of the same order of magnitude as that inferred from the diffusion coefficient of singlet excitons in a molecular crystal, such as anthracene at room temperature.[38] Despite this consistency one should consider the applicability of Eq. (24) for determining a Förster radius with some caution since in conjugated polymers the size of an exciton is of order of two repeat units[39] and, hence, longer than a typical site-to-site intrachain spacing.

When comparing computed and experimental decay patterns in double logarithmic representation, one notices that, notably in the PPPV systems, turnover to stretched exponential behavior occurs earlier than predicted by simulation. This is to be expected since in the polymer the distances among the chromophores are not identical as in the computer model but subject to some

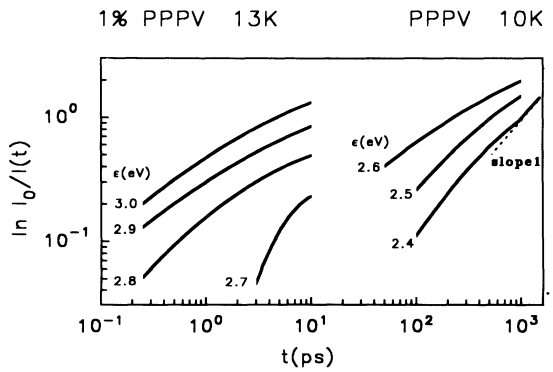

FIG. 11. Smoothed PL decay curves for PPPV/PC and PPPV taken from Figs. 4 and 5, respectively, plotted on a double logarithmic $\ln I_0/I(t)$ versus time scale.

distribution, the more so the more disordered the system is in topological terms. One necessary consequence is that even nearest-neighbor transfer acts will be subject to a distribution of rates equivalent to an erosion of the experimental decay pattern at short times. The bulky phenyl substituent in PPPV will enhance this effect as compared to PPV.

It is worth pointing out that the general decay pattern of PL does not change as the detection energy is swept across the localization energy at the tail of the DOS inferred earlier from site-selective cw PL spectra. The fact that the dependence of t_0 on detection energy is in good agreement with the prediction of the concept of excitation hopping within a manifold of states that are all localized represents another strong argument in favor of the applicability of the latter.

Any alternative model for interpreting the present experimental data had to invoke a time-dependent nonradiative pathway for deactivating an excited state that not only depends on the energy of a given state but also on the energy of that state relative to the center of the inhomogeneously broadened $S_1 \leftarrow S_0$ 0-0 transition. This leads to an inconsistency. On the basis of a linear variation of the transition energy with reciprocal chain lengths[13] one would estimate that in PPPV L_{eff} ranges between 5 and 8 while in PPV it is approximately twice as large. If a hypothetical nonradiative decay channel other than energy migration became slower upon increasing the chain length one would expect it to be much less efficient in PPV as compared to PPPV. Within the energy migration concept, on the other hand, it is the statistical spread of the chain length that matters rather than its absolute value since the quantity that controls relaxation is the width of the DOS rather than the location of its center on an absolute energy scale. Moreover, a non-transport-based relaxation concept would be unable to account for the accumulation of excitations within the tail of the DOS.

V. CONCLUDING REMARKS

We have demonstrated that the spectrally resolved temporal decay of the photoluminescence of PPV-related conjugated polymers can consistently be described in terms of an incoherent random walk of neutral excitations migrating via dipole-dipole coupling among subunits of the chain that constitute the elementary absorbers of the systems in the sense of molecular spectroscopy. The time scale of the elementary act bears out a Förster radius of $R_0 \approx 18$ Å consistent with what is to be expected for chemically identical, i.e., spectrally weakly overlapping chromophores. The energy-dependent relaxation profiles show pronounced deviations from the KWW law. These are mainly due to the *nonrandom* arrangement of the sites along the polymer chain which produces pathological spectra of hopping modes as has been shown by simulation experiments. At longer times the decay behavior approaches a stretched exponential behavior with a limiting value $\beta = 0.4$ reflecting energy transport in a random system. The variation of the time frame of the decay with detection energy within the zero vibronic component of the inhomogeneously broadened $S_1 \leftarrow S_0$ transition is a signature of the energetic relaxation of excitations within the density of localized hopping states. The long-time decay is determined by the intrinsic lifetime of a PPV-chain segment which turns out to be virtually the same as that of an oligomer consisting of three phenyl rings. This indicates that the spatial extent of the excited state wave function does not exceed that of the oligomer, i.e., it is less than the effective conjugation length of PPV. Otherwise the oscillator strength should be larger, resulting in a reduction of the radiative lifetime. All observed features are independent of excitation power indicating that no bimolecular effects are important. In summary, the results clearly demonstrate that the elementary optical excitations determining the emission properties in these systems are neutral rather than charged entities.

ACKNOWLEDGMENTS

This work has been supported by Deutsche Forschungsgemeinschaft, Fonds zur Förderung der wissenschaftlichen Forschung, Wien, Österreich (B.M., H.F.K., P8775-PHY), Stiftung Volkswagenwerk, and Alfried Krupp Stiftung which are gratefully acknowledged. We thank M. Gailberger and A. Greiner for preparing PPV and PPPV.

[1] A. J. Heeger, S. Kivelson, R. J. Schrieffer, and W. P. Su, Rev. Mod. Phys. **60**, 781 (1988).
[2] L. Lauchlan, S. Etemad, T. C. Chung, A. J. Heeger, and A. G. Mac Diarmid, Phys. Rev. B **24**, 3701 (1981).
[3] H. H. Hörhold, M. Helbig, D. Raabe, J. Opfermann, U. Scherf, R. Stockmann, and D. Weiss, Z. Chem. **27**, 126 (1987).
[4] T. Tagiguchi, D. H. Park, H. Ueno, K. Yoshino, and P. Sujimoto, Synth. Met. **17**, 637 (1989).
[5] C. H. Lee, G. Yu, and A. J. Heeger, Phys. Rev. B **47**, 15 543 (1993).
[6] K. Fesser, A. R. Bishop, and D. K. Campbell, Phys. Rev. B **27**, 4804 (1983).
[7] Z. Vardeny, E. Ehrenfreund, O. Brafman, M. Novak, H. Schaffer, A. J. Heeger, and F. Wudl, Phys. Rev. Lett. **56**, 671 (1986).
[8] R. H. Friend, D. D. C. Bradley, and P. D. Townsend, J. Phys. D **20**, 1367 (1987).
[9] D. Birnbaum and B. E. Kohler, J. Chem. Phys. **90**, 3506 (1989); **95**, 4783 (1991).
[10] N. Periasamy, R. Danieli, G. Ruani, R. Zambioni, and C. Taliani, Phys. Rev. Lett. **68**, 919 (1992).
[11] K. Pichler, D. A. Halliday, D. D. C. Bradley, P. L. Burn, R. H. Friend, and A. B. Holmes, J. Phys. Condens. Matter **5**, 7155 (1993).
[12] H. Rauscher, H. Bässler, D. D. C. Bradley, and M. Hen-

necke, Phys. Rev. B **42**, 9830 (1990).
[13] S. Heun, R. F. Mahrt, A. Greiner, U. Lemmer, H. Bässler, D. A. Halliday, D. D. C. Bradley, P. L. Burn, and A. B. Holmes, J. Phys. Condens. Matter **5**, 247 (1993).
[14] S. Mukamel and H. X. Wang, Phys. Rev. Lett. **69**, 65 (1992).
[15] S. Abe, M. Schreiber, and W. P. Su, Phys. Rev. B **45**, 9432 (1992).
[16] J. M. Leng, S. Jeglinski, X. Wei, R. E. Benner, and Z. V. Vardeny, Phys. Rev. Lett. **72**, 156 (1994).
[17] M. Yan, L. J. Rothberg, F. Papdimitrakopoulos, M. E. Galvin, and T. M. Miller, Phys. Rev. Lett. **72**, 1104 (1994).
[18] X. Q. Zhou, G. C. Cho, U. Lemmer, W. Kütt, K. Wolter, and H. Kurz, Solid State Electron. **32**, 1591 (1989).
[19] T. Elsässer, J. Shah, L. Rota, and P. Lugli, Phys. Rev. Lett. **66**, 1757 (1991).
[20] B. Movaghar, M. Grünewald, B. Ries, H. Bässler, and D. Würtz, Phys. Rev. B **33**, 5345 (1986).
[21] U. Lemmer, R. F. Mahrt, Y. Wada, A. Greiner, H. Bässler, and E. O. Göbel, Chem. Phys. Lett. **209**, 243 (1993).
[22] R. Kersting, U. Lemmer, R. F. Mahrt, K. Leo, H. Kurz, H. Bässler, and E. O. Göbel, Phys. Rev. Lett. **70**, 3820 (1993).
[23] U. Lemmer, R. F. Mahrt, Y. Wada, A. Greiner, H. Bässler, and E. O. Göbel, Appl. Phys. Lett. **62**, 2827 (1993).
[24] B. Mollay and H. F. Kauffmann, Chem. Phys. **177**, 645 (1993).
[25] B. Mollay and H. F. Kauffmann, in *Disorder Effects on Relaxational Processes*, edited by R. Richert and A. Blumen (Springer, Berlin, 1994), p. 505.
[26] B. Mollay and H. F. Kauffmann, Macromolecules (to be published).
[27] J. Shah, IEEE J. Quantum Electron. **24**, 276 (1988); H. Mahr and M. D. Hirsch, Opt. Commun. **13**, 96 (1975).
[28] T. Förster, Z. Naturforsch. Teil A **4**, 321 (1949).
[29] W. H. Press, B. P. Flannery, S. A. Teukolsky, and W. T. Vetterling, *Numerical Recipes, The Art of Scientific Computing* (Cambridge University Press, Cambridge, 1986).
[30] R. Richert, H. Bässler, B. Ries, B. Movaghar, and M. Grünewald, Philos. Mag. Lett. **59**, 95 (1989).
[31] G. Williams, Adv. Polym. Sci. **33**, 59 (1979).
[32] J. Klafter and M. F. Shlesinger, Proc. Natl. Acad. Sci. U.S.A. **83**, 848 (1986); J. Klafter and A. Blumen, Chem. Phys. Lett. **119**, 377 (1985).
[33] R. G. Palmer, D. L. Stein, E. Abrahams, and P. W. Anderson, Phys. Rev. Lett. **53**, 953 (1984); J. Budimir and J. L. Skinner, J. Chem. Phys. **82**, 5253 (1985).
[34] A. Blumen, G. Zumofen, and J. Klafter, Phys. Rev. B **30**, 5379 (1984); J. Klafter and A. Blumen, J. Chem. Phys. **80**, 875 (1984); *Transport and Relaxation in Random Materials*, edited by J. Klafter, R. J. Rubin, and M. F. Shlesinger (World Scientific, Singapore, 1985); B. Mollay and H. F. Kauffmann, J. Chem. Phys. **97**, 4380 (1992).
[35] T. Damerau, M. Hennecke, and A. Greiner, Polym. Bull. (to be published).
[36] A. Ochse, U. Lemmer, M. Deussen, J. Feldmann, A. Greiner, R. F. Mahrt, H. Bässler, and E. O. Göbel, Mol. Cryst. Liq. Cryst. (to be published).
[37] I. B. Berlman, *Handbook of Fluorescence Spectra of Aromatic Molecules*, 2nd ed. (Academic Press, New York, 1971).
[38] M. Pope and C. E. Swenberg, *Electronic Processes in Molecular Crystals* (Clarendon Press, Oxford, 1982).
[39] A. Horvath, H. Bässler, and G. Weiser, Phys. Status Solidi B **173**, 755 (1982).